Structural Engineering and Mechanics, Vol. 4, No. 6 (1996) 631-644
DOI: http://dx.doi.org/10.12989/sem.1996.4.6.631

Micro/macro properties of geomaterials: a homogenization method for viscoelastic problem

Yasuaki Ichikawa†

Department of Geotechnical and Environmental Engineering Nagoya University, Nagoya 464-01, Japan

Jianguo Wang‡

Department of Civil Engineering, National University of Singapore, 119260 Singapore

Gyo-Cheol Jeong‡†

Department of Geology, Andong National University, Andong 760-749, Korea

Abstract. Geomaterials such as soil and rock are composed of discrete elements of microstructures with different grains and microcracks. The studies of these microstructures are of increasing interest in geophysics and geotechnical engineering relating to underground space development. We first show experimental results undertaken for direct observation of microcrack initiation and propagation by using a newly developed experimental system, and next a homogenization method for treating a viscoelastic behavior of a polycrystalline rock.

Key words: granite; microscope observation; homogenization method; visco-elastic problem.

1. Introduction

Granitic rock involves microstructures including not only crystal grains but also cracks and cavities whose evolution and interaction, called the microdamaging process, determine their macroscopic mechanical response. Thus, it is a complex composite with microcstructures which are caused by different geologic processes and under varying conditions.

Numerous recent studies have shown that the physical properties of rocks are not only affected by the constituent minerals (Olsson 1974, Wong 1990) and their preferred orientation (Kern *et al.* 1985) but also by the microcracks (Bombolakis 1973, Kranz 1979a, b, Yukutake 1989, Ahrens *et al.* 1993).

In this study, we first show experimental results undertaken for direct observation of microcrack initiation and propagation by using a newly developed experimental system. From the experimental results, it is considered that the true damage process up to the peak stress was found to involve four stages:

1) pre-existing microcrack closure,
2) dilatancy and the associated microcracking,

† Ph.D, Associate Professor
‡ Ph.D, Post-Graduate Research Fellow
‡† Associate Professor

3) clustering microcracks, and
4) microcrack localization.

More detailed observations indicate that microdamage is initiated at contact portion of two grains. Furthermore damaging process of micro- to macro-scale are clearly observed, and the shear localization and faulting with microcracking are clarified.

Second a viscoelastic homogenization theory is applied to analyze the micro and macro level of stress distribution in a crystalline rock which is a composite material of some minerals. It is assumed that the microstructure is periodic, and each mineral of the rock shows a viscoelastic property. We call one periodic structure as a unit cell in the homogenization theory.

2. Experiments

The microcrack formation and subsequent damage propagation were examined in a series of compression test by using coarse-grained granite under nominally dried condition at room temperature.

2.1. Experimental procedures

Specimens of coarse-grained granite from Geochang, Korea are consisted mainly of 36.5% quartz, 56.3% feldspar and 7.2% biotite (modal test results). The bulk density and apparent porosity of the granite are 2.58 g/cm^3 and 0.83%, respectively. The dimension of specimens is shown in Fig. 1.

The design of the specimen assembly and experimental system, consisting of three subsystems, i.e., a) loading system, b) data-recording system and c) observation system, are illustrated in Fig. 2. The granite specimen with a strain gauge was placed on a concave-shaped steel block in a loading vessel, and stress was applied to the specimen by a piston actuated through manually controlled loading pump (see Fig. 2). Axial stress and strain were recorded in a personal computer.

In order to observe the initiation and growth pattern of microcracks directly, a stereoscopic microscope (Nikon, SMZ-U) is used. A video monitoring system was used for continuous recording and a still camera was provided for intermittent recording.

2.2. Microscopic observations

Microcracks which consist of healed cleavages, pre-existing intracrystalline microcracks and

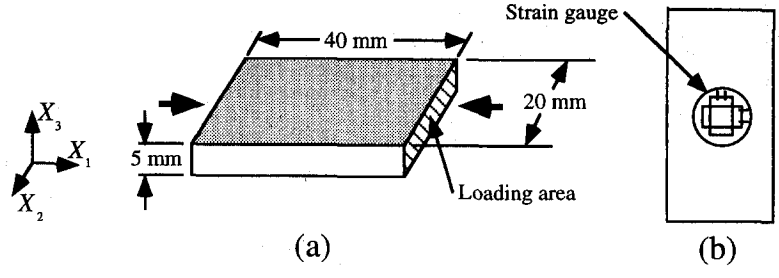

Fig. 1 (a) Dimensions of specimen; the direction of compression is parallel to X_1, and (b) the location of strain gauge.

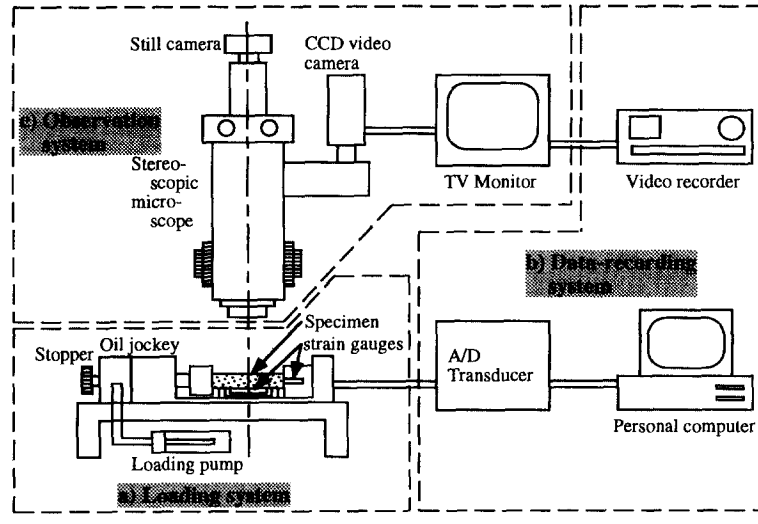

Fig. 2 Experimental system; (a) loading unit, (b) data-recording unit, and (c) observational unit.

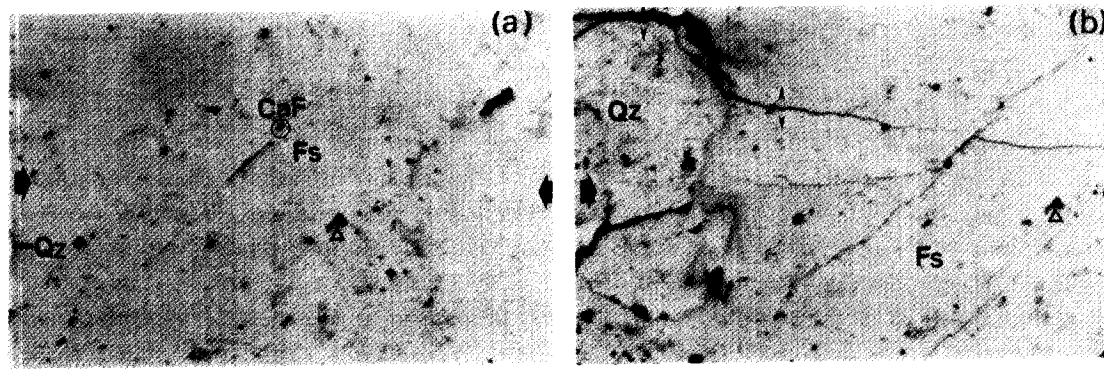

Fig. 3 Photomicrograph showing initiation and propagation of microcracks at quartz(Qz)-feldspar(Fs) contact portion; (a) no loading and (b) 80 MPa. Axial stress direction is horizontal, and the open triangle marks the same point.

grain boundary microcracks were traced on stereoscopic photomicrographs under gradually increased stress at the various portions of the specimen.

Before specimens are loaded, many healed pre-existing microcracks (marks CrQ in Fig. 3(b)) are observed in quartz grains, and some longish microcavities (marks CaF in Fig. 3(a)) with blunt ends are observed in feldspar.

In quartz grains contained in granite specimens, pre-existing itracrystalline microcracks are well developed in various direction, but microcracks in feldspar and biotite grains were few. The higher microcrack densities within quartz grains as compared to adjacent feldspar grains may indicate that the initiation of microcracking is generally related to internal stresses or difference of volumetric strains at grain scale.

Nur, *et al.* (1970) reported that quartz grain in granite underwent a large volume change upon cooling from 600℃. Therefore, the existence of these pre-existing microcracks is mainly due to the difference of thermo-mechanical properties of minerals (see Table 1).

Table 1 Physical properties of quartz and feldspar (Skinner 1966, Birch 1961)

Minerals	$\alpha(\times 10^{-5}\ ^{\circ}C^{-1})$	$K(\times 10^{4}$ MPa)	$\beta(TPa^{-1})$
Quartz	5.15	3.82	26.2
Feldspar	1.45	4.29	23.3

α: thermal expansion coefficient, K: bulk modulus, β: compressibility

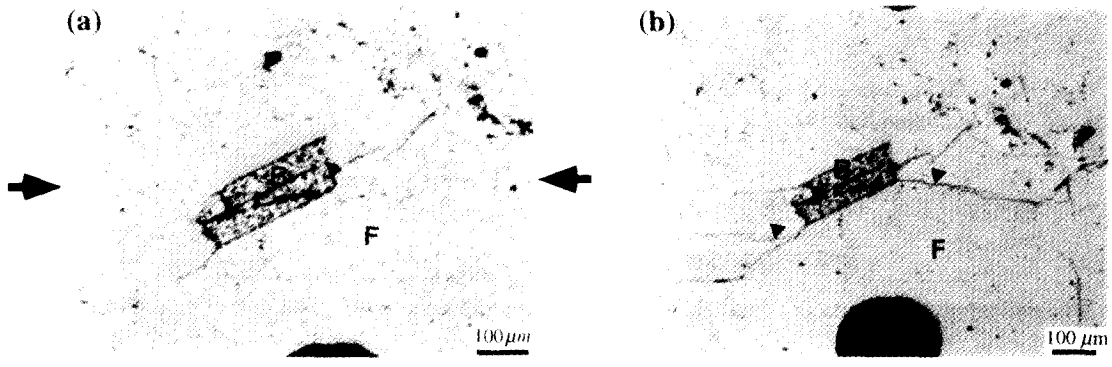

Fig. 4 Photomicrograph showing initiation and propagation of microcracks at biotite(B)-feldspar(F) contact portion; (a) no loading and (b) 45 MPa. Axial stress direction is horizontal.

The grain boundaries of granite used in this study which mostly consist of coarse-grained quartz, feldspar and biotite are observed to be open. The location of stress-induced microdamage initiation, growth direction and the relationship between pre-existing microcracks and stress-induced microcracks were observed in great detail by using the stereoscopic microscope which enables us to observe continuously during loading.

The primary intracrystalline microcrack, that is, the cleavage microcrack in feldspar grains is initiated through the defective cleavage (CaF in Fig. 3(a)) at a stress level 30 MPa. At the same time, microcavities are linked, and intracrystalline microcracks and grain boundary microcracks parallel or subparallel to the axial stress direction are predominantly caused by tensile stress due to Poisson effect. Furthermore local variations in elastic properties of different minerals or the presence of microcracks cause the stress to be concentrated and the remote compressive stresses are converted to locally tensile stresses. Based on these facts, intracrystalline microcracks nearly parallel to the axial stress direction are initiated from pre-existing grain boundary microcracks between quartz and feldspar grain. Note that the compressibility of feldspar is lower than that of quartz grain (Table 1). On the other hand, microcracks perpendicular and inclined to the axial stress direction are closed and sheared, respectively.

Cleavage microcracks which are parallel to {001} are common in biotite. Localized shear strains of granitic rocks and ductile shear zones are frequently associated with the presence of biotite. Shear stresses resolved on {001} cleavage planes of most biotite grains were large and microstructures developed within biotite suggest that frictional sliding on cleavage planes was important (Fig. 4). In addition, frictional sliding seems to be developed along the interfaces between biotite and surrounding feldspar grains. Displacement along grain boundary microcracks increases as the axial strain increases. The end of these microcracks sometimes shows complicated geometry with many fractions.

3. Homogenization analysis for viscoelastic material

The homogenization theory (Sanchez-Palencia 1980) allows us to determine a microscopic stress distribution for a composite material which has a periodic structure in microscale. We here propose a homogenization theory for viscoelastic material under a Laplace transformation. The scheme is shown in Fig. 5.

3.1. Viscoelastic problem in Laplace space

Let us suppose a material body with a microscale periodic structure (Fig. 6). If the material is viscoelastic, the corresponding equations in a Laplace transformation space are given as follows:

(Governing equation)

$$\frac{\partial \hat{\sigma}_{ij}^{\varepsilon}}{\partial x_j}+\hat{f}_i^{\varepsilon}=0 \text{ in } \Omega^{\varepsilon} \tag{1}$$

(Boundary conditions)

$$\hat{u}_i^{\varepsilon}=\hat{\bar{u}}_i \text{ on } \Gamma_u \tag{2}$$

$$\hat{\sigma}_{ij}^{\varepsilon} n_j=\hat{\bar{t}}_i \text{ on } \Gamma_f \tag{3}$$

where

$$\hat{\sigma}_{ij}^{\varepsilon}(\mathbf{x},\ p)=\int_0^{\infty} \hat{\sigma}_{ij}^{\varepsilon}(\mathbf{x},\ t)\exp(-pt)\,dt$$

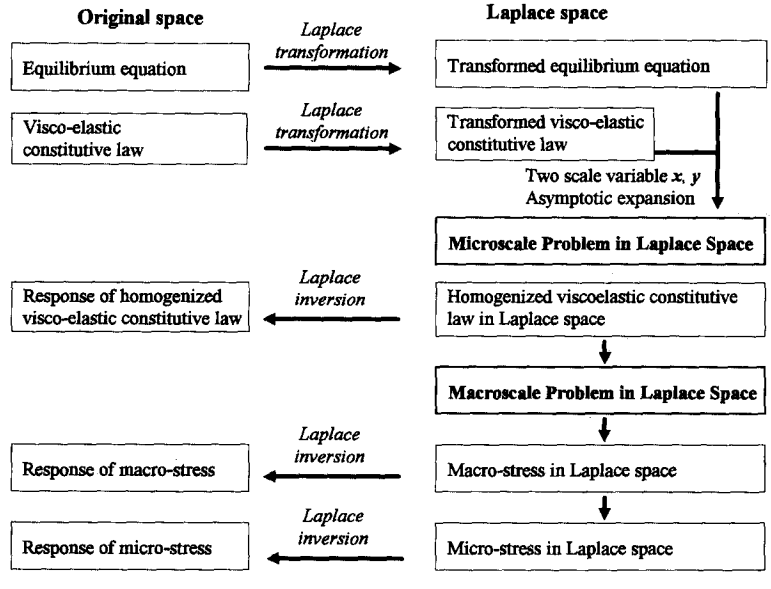

Fig. 5 Scheme of homogenization analysis for viscoelastic problem.

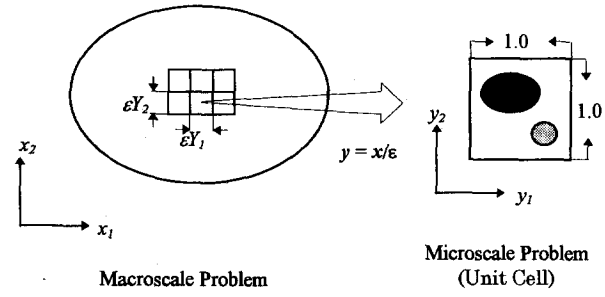

Fig. 6 Material body with a periodic microstructure.

is the Laplace transformed stress. Similarly, $\hat{u}_i^{\varepsilon}$ and $\hat{f}_i^{\varepsilon}$ (x, p) are the Laplace transformed displacement and body force, respectively.

(Initial condition)

$$[u_i^{\varepsilon}(\boldsymbol{x}, t=0)]=\hat{\bar{u}}_i^{0}(\boldsymbol{x}) \tag{4}$$

(Strain-displacement relation)

$$\hat{\varepsilon}_{ij}^{\varepsilon}(\hat{\boldsymbol{u}}^{\varepsilon})=\frac{1}{2}\left(\frac{\partial \hat{u}_i^{\varepsilon}}{\partial x_j}+\frac{\partial \hat{u}_j^{\varepsilon}}{\partial x_i}\right) \tag{5}$$

(Constitutive relation)

$$\hat{\sigma}_{ij}^{\varepsilon}(p)=p(2\hat{G}\hat{\varepsilon}_{ij}^{\varepsilon}+\hat{\lambda}\hat{\varepsilon}_{rs}^{\varepsilon}\delta_{rs}\delta_{ij})=p\hat{D}_{ijrs}\hat{\varepsilon}_{rs}^{\varepsilon}=\hat{M}_{ijrs}\hat{\varepsilon}_{rs}^{\varepsilon} \tag{6}$$

where

$$\hat{\lambda}(p)=\hat{K}(p)-\frac{2}{3}\hat{G}(p),\ \hat{G}(p)=\frac{G_0}{p}+\sum_{i=1}^{n}\frac{G_i}{p+(1/\tau_i^{s})},\ \hat{K}(p)=\frac{K_0}{p}+\sum_{i=1}^{n}\frac{K_i}{p+(1/\tau_i^{v})}$$

Note that τ_i^{s} and τ_i^{v} are the shearing and volumetric relaxation times, respectively, and the Maxwell model corresponding to Eq. (6) in the original space is written as

$$\sigma^{\varepsilon}(t)=2\int_{-\infty}^{t}G(t-s)\frac{d\boldsymbol{e}^{\varepsilon}}{ds}ds+3\int_{-\infty}^{t}\lambda(t-s)\frac{d\bar{\varepsilon}^{\varepsilon}}{ds}ds$$

$$\bar{\varepsilon}_{ij}^{\varepsilon}=\frac{1}{3}\varepsilon_{kk}^{\varepsilon}\delta_{ij},\ \boldsymbol{e}_{ij}^{\varepsilon}=\varepsilon_{ij}^{\varepsilon}-\bar{\varepsilon}_{ij}^{\varepsilon} \tag{7}$$

3.2. Microscale and macroscale problems in Laplace space

Let us introduce an asymptotic expansion for $\hat{\boldsymbol{u}}^{\varepsilon}$ in terms of $\varepsilon=\boldsymbol{x}/\boldsymbol{y}$.

$$\hat{u}_i^{\varepsilon}(\boldsymbol{x}, p)=\hat{u}_i^{0}(\boldsymbol{x}, \boldsymbol{y}, p)+\varepsilon\hat{u}_i^{1}(\boldsymbol{x}, \boldsymbol{y}, p)+\varepsilon^2\hat{u}_i^{2}(\boldsymbol{x}, \boldsymbol{y}, p)+\cdots \tag{8}$$

Here

$$\hat{u}_i^{\alpha}(\boldsymbol{x}, \boldsymbol{y}, p)=\hat{u}_i^{\alpha}(\boldsymbol{x}, \boldsymbol{y}+\boldsymbol{Y}, p)\ (\alpha=0, 1, 2, \cdots) \tag{9}$$

are Y-periodic funtions. Note that the global coordinate $\boldsymbol{x}$ is called a 'slow' spacial variable,

and the local one $\boldsymbol{y}$ a 'fast' spacial variable.

Since $\boldsymbol{y}=\boldsymbol{x}/\varepsilon$ and ε approaches to zero, the partial differential operator is transformed as

$$\frac{\partial}{\partial x_i} \Rightarrow \frac{\partial}{\partial x_i}+\frac{1}{\varepsilon}\frac{\partial}{\partial y_i} \tag{10}$$

Substituting this into Eq. (5) yields

$$\hat{\varepsilon}_{ij}^{\varepsilon}(\boldsymbol{x},\ p)=\frac{1}{\varepsilon}\hat{\varepsilon}_{ij}^{0y}+(\hat{\varepsilon}_{ij}^{0x}+\hat{\varepsilon}_{ij}^{1y})+\varepsilon(\hat{\varepsilon}_{ij}^{1x}+\hat{\varepsilon}_{ij}^{2y})+\cdots$$

$$\hat{\varepsilon}_{ij}^{0y}=\frac{1}{2}\left(\frac{\partial \hat{u}_i^{\,0}}{\partial y_j}+\frac{\partial \hat{u}_j^{\,0}}{\partial y_i}\right),\ \hat{\varepsilon}_{ij}^{0x}=\frac{1}{2}\left(\frac{\partial \hat{u}_i^{\,0}}{\partial x_j}+\frac{\partial \hat{u}_j^{\,0}}{\partial x_i}\right),\ \hat{\varepsilon}_{ij}^{1y}=\frac{1}{2}\left(\frac{\partial \hat{u}_i^{\,1}}{\partial y_j}+\frac{\partial \hat{u}_j^{\,1}}{\partial y_i}\right)$$

$$\hat{\varepsilon}_{ij}^{1x}=\frac{1}{2}\left(\frac{\partial \hat{u}_i^{\,1}}{\partial x_j}+\frac{\partial \hat{u}_j^{\,1}}{\partial x_i}\right),\ \hat{\varepsilon}_{ij}^{2y}=\frac{1}{2}\left(\frac{\partial \hat{u}_i^{\,2}}{\partial y_j}+\frac{\partial \hat{u}_j^{\,2}}{\partial y_i}\right) \tag{11}$$

By using the constitutive relation given by Eq. (6) we have

$$\hat{\sigma}_{ij}^{\varepsilon}(\boldsymbol{x},\ \boldsymbol{y},\ p)=\frac{1}{\varepsilon}\hat{\sigma}_{ij}^{0}+\hat{\sigma}_{ij}^{1}+\varepsilon\hat{\sigma}_{ij}^{2}+\cdots$$

$$\hat{\sigma}_{ij}^{0}=\hat{M}_{ijkl}\hat{\varepsilon}_{kl}^{0y},\ \hat{\sigma}_{ij}^{1}=\hat{M}_{ijkl}(\hat{\varepsilon}_{kl}^{0x}+\hat{\varepsilon}_{kl}^{1y}),\ \hat{\sigma}_{ij}^{2}=\hat{M}_{ijkl}(\hat{\varepsilon}_{kl}^{1x}+\hat{\varepsilon}_{kl}^{2y}) \tag{12}$$

The governing Eq. (1) is then written as

$$\frac{1}{\varepsilon^2}\frac{\partial \hat{\sigma}_{ij}^{0}}{\partial y_j}+\frac{1}{\varepsilon}\left[\frac{\partial \hat{\sigma}_{ij}^{0}}{\partial x_j}+\frac{\partial \hat{\sigma}_{ij}^{1}}{\partial y_j}\right]+\left[\frac{\partial \hat{\sigma}_{ij}^{1}}{\partial x_j}+\frac{\partial \hat{\sigma}_{ij}^{2}}{\partial y_j}\right]+\cdots=-\hat{f}_i^{\varepsilon}(\boldsymbol{x},\ \boldsymbol{y},\ p) \tag{13}$$

Each term for $\varepsilon^{\alpha}(\alpha=-2,\ -1,\ 0,\ 1,\ \cdots)$ must be zero as $\varepsilon\to 0$, so we have the following identities:

$O(\varepsilon^{-2})$ **term**;

$$\frac{\partial \hat{\sigma}_{ij}^{0}}{\partial y_j}=0 \tag{14}$$

This implies that $\hat{\sigma}_{ij}^{0}(\boldsymbol{x},\ \boldsymbol{y},\ p)=\hat{\sigma}_{ij}^{0}(\boldsymbol{x},\ p)$, and we will be able to set $\hat{\sigma}_{ij}^{0}=0$ because the term ε^{-1} must be bounded as $\varepsilon\to 0$. Thus, we have $\hat{u}_i^{\,0}(\boldsymbol{x},\ \boldsymbol{y},\ p)=\hat{u}_i^{\,0}(\boldsymbol{x},\ p)$. Under this condition, the strain given by Eq. (11) is approximated as

$$\hat{\varepsilon}_{ij}^{\varepsilon}\simeq\hat{\varepsilon}_{ij}^{0x}+\hat{\varepsilon}_{ij}^{1y} \tag{15}$$

$O(\varepsilon^{-1})$ **term** (Microscale equation);

The terms of $O(\varepsilon^{-1})$ in Eq. (13) together with the condition $\hat{\sigma}_{ij}^{0}=0$ are given by

$$\frac{\partial \hat{\sigma}_{ij}^{1}}{\partial y_j}=0 \tag{16}$$

Recalling the constitutive Eq. (6), we have

$$\frac{\partial}{\partial y_j}\{\hat{M}_{ijrs}(\boldsymbol{y},\ p)\,[\hat{\varepsilon}_{rs}^{0x}(\boldsymbol{x};\ p)+\hat{\varepsilon}_{rs}^{1y}(\boldsymbol{x},\ \boldsymbol{y};\ p)]\}=0 \tag{17}$$

where

$$\hat{M}_{ijkl}(\boldsymbol{y},\ p)=D^0_{ijrs}(\boldsymbol{y})+p\hat{D}^1_{ijrs}(\boldsymbol{y},\ p)$$

$$D^0_{ijrs}=2G_0\,\delta_{ri}\,\delta_{sj}+\lambda_0\,\delta_{ij}\,\delta_{rs},\ \hat{D}^1_{ijrs}(p)=2\left\{\sum_{i=1}^{n}\frac{\hat{G}_i(p)}{p+1/\tau_i^s}\right\}\delta_{ri}\,\delta_{sj}+\left\{\sum_{i=1}^{n}\frac{\hat{\lambda}_i(p)}{p+1/\tau_i^v}\right\}\delta_{ij}\,\delta_{rs}$$

Now we define a characteristic function $\hat{\chi}_i^{kl}(\boldsymbol{y},\ p)$ in the unit cell as

$$\hat{u}_i^1(\boldsymbol{x},\ \boldsymbol{y},\ p)=-\hat{\chi}_i^{kl}(\boldsymbol{y},\ p)\frac{\partial\hat{u}_k^0}{\partial x_l}+C_i(\boldsymbol{x}) \tag{18}$$

where $C_i(\boldsymbol{x})$ is a constant with respect to $\boldsymbol{x}$. Substituting this into Eq. (17), we have the following microscale or unit cell problem:

$$\frac{\partial}{\partial y_j}\left\{\hat{M}^1_{ijrs}(\boldsymbol{y};\ p)\left(\delta_{rk}\,\delta_{sl}-\frac{\partial\hat{\chi}_k^{rs}}{\partial y_l}\right)\right\}=0 \tag{19}$$

A weak form of this equation which can be solved by introducing an appropriate approximation method is then given by

$$\int_Y\hat{M}_{ijkl}\frac{\partial\hat{\chi}_k^{rs}}{\partial y_l}\ \frac{\partial v_i}{\partial y_j}dy=\int_Y\hat{M}_{ijrs}\frac{\partial v_i}{\partial y_j}dy\qquad\forall v_i(v_i=0\ \text{on the unit cell boundary}\ \partial Y) \tag{20}$$

$O(\varepsilon^0)$ term (Macroscale equation);

The terms of $O(\varepsilon^0)$ in Eq. (13) are now given by

$$\frac{\partial\hat{\sigma}_{ij}^1}{\partial x_j}+\frac{\partial\hat{\sigma}_{ij}^2}{\partial y_j}+\hat{f}_i^e(\boldsymbol{x},\ \boldsymbol{y},\ p)=0 \tag{21}$$

Let us introduce an averaging operator for the unit cell $\boldsymbol{Y}$ by

$$\langle\bullet\rangle=\frac{1}{|\boldsymbol{Y}|}\int_Y\bullet dy$$

The second term of Eq. (21) under this averaging operation vanishes because of the periodicity of $\hat{\sigma}_{ij}^2$:

$$\left\langle\frac{\partial\hat{\sigma}_{ij}^2}{\partial y_j}\right\rangle=\frac{1}{|\boldsymbol{Y}|}\int_Y\frac{\partial\hat{\sigma}_{ij}^2}{\partial y_j}dy=\frac{1}{|\boldsymbol{Y}|}\int_{\partial Y}\hat{\sigma}_{ij}^2n_jd\Gamma=0$$

Thus we have the macroscale equation such that

$$\frac{\partial\langle\hat{\sigma}_{ij}^1\rangle}{\partial x_j}+\langle\hat{f}_i^s\rangle=0 \tag{22}$$

The boundary condition and constitutive equation are also averaged as

$$\langle\hat{u}_i^0\rangle=\langle\hat{\bar{u}}_i\rangle\quad\text{on}\quad\Gamma_u \tag{23}$$

$$\langle\hat{\sigma}_{ij}^1\rangle=\hat{M}^h_{ijrs}\hat{\varepsilon}_{rs}^{0x}(p)$$

$$\hat{M}^h_{ijkl}=\frac{1}{|\boldsymbol{Y}|}\int_Y\hat{M}_{ijrs}\left[\delta_{rk}\,\delta_{ls}-\frac{\partial\hat{\chi}_k^{rs}}{\partial y_l}\right]dy \tag{24}$$

3.3. Inverse Laplace transformation for stresses

Let ε of $y=x/\varepsilon$ be small enough, so the periodic structure is independent from the elapsed time. Then we can assume that

$$\begin{aligned}\langle\hat{\sigma}_{ij}^{1}\rangle &= \langle\hat{M}^{1}_{ijkl}(p)\rangle\,[\hat{\varepsilon}_{kl}^{0x}(p)+\hat{\varepsilon}_{kl}^{1y}(p)]\\ &= \langle[D^{0}_{ijkl}+p\,\hat{D}^{1}_{ijkl}(p)]\,[\hat{\varepsilon}_{kl}^{0x}(p)-\frac{\partial\chi_k^{rs}}{\partial y_l}\,\hat{\varepsilon}_{rs}^{0x}(p)]\rangle\\ &= \left\langle D^{0}_{ijkl}\left(\delta_{ik}\delta_{jl}-\frac{\partial\chi_k^{rs}}{\partial y_l}\right)\right\rangle\hat{\varepsilon}_{rs}^{0x}(p)+\left\langle pD^{1}_{ijkl}\left(\delta_{ik}\delta_{jl}-\frac{\partial\chi_k^{rs}}{\partial y_l}\right)\right\rangle\hat{\varepsilon}_{kl}^{0x}\end{aligned} \tag{25}$$

And the inverse transformation gives

$$\langle\sigma_{ij}^{1}\rangle=\langle\sigma_{ij}^{10}\rangle+\langle\sigma_{ij}^{11}\rangle$$

$$\langle\sigma_{ij}^{10}\rangle=\left\langle D^{0}_{ijkl}\left(\delta_{ik}\delta_{jl}-\frac{\partial\chi_k^{rs}}{\partial y_l}\right)\right\rangle\varepsilon_{rs}^{0x}(t),\quad \langle\sigma_{ij}^{11}\rangle=\int_0^t\left\langle D^{1}_{ijkl}(t-s)\left(\delta_{ik}\delta_{jl}-\frac{\partial\chi_k^{rs}}{\partial y_l}\right)\right\rangle\frac{d\varepsilon_{rs}^{0x}}{ds}\,ds \tag{26}$$

Here $\langle\sigma_{ij}^{10}\rangle$ represents an instantaneous elastic term, and $\langle\sigma_{ij}^{11}\rangle$ a time dependent Maxwell term. Similarly, the stress in micro level can be given as

$$\sigma_{ij}^{1}=D^{0}_{ijkl}\left(\delta_{ik}\delta_{jl}-\frac{\partial\chi_k^{rs}}{\partial y_l}\right)\varepsilon_{rs}^{0x}(t)+\int_0^t D^{1}_{ijkl}(t-s)\left(\delta_{ik}\delta_{jl}-\frac{\partial\chi_k^{rs}}{\partial y_l}\right)\frac{d\varepsilon_{rs}^{0x}}{ds}\,ds \tag{27}$$

Note on the Schapery's collocation method

The stress under a relaxation test and the strain under a creep test are monotonically decaying and increasing functions, respectively. These kind of functions can be represented as a sum of exponential functions ($\exp(-\alpha x)$). Schapery (1961) proposed an inverse Laplace transformation method which is applicable to this type of functions.

Based on an irreversible thermodynamic theory, Schapery assumed that if a step function of excitation is input at $t=0$, the response $y(t)$ such as stress and viscoelastic coefficients can be represented as

$$y(t)=a_1-f(t)$$

where a_1 is a constant determined by the initial condition, and $f(t)$ is a transient part which is of the form

$$f(t)=\int_0^\infty F(\alpha)\,e^{-t/\alpha}\,d\alpha$$

Note that $F(\alpha)$ is called a distribution function. This $f(t)$ can be approximated as a Dirichlet series such that

$$f_D(t)=\sum_{i=1}^{n}S_i e^{-t/\tau_i} \tag{28}$$

where $\tau_i>0$ are points which are given a priori, and S_i are unknown parameters.

Schapery (1961) states that the square error between $f(t)$ and $f_D(t)$ becomes minimum if $f(p)$ coincides with $\hat{f}_D(p)$ at the designated points $p=1/\tau_i (i=1, 2, \cdots, n)$. This is understood as follows: Let us define a square error by

$$E=\frac{1}{2}\int_0^\infty [f(t)-f_D(t)]^2 dt \tag{29}$$

Substituting Eq. (31) into the above and minimizing the error for the unknown parameters $S_i (i=1, 2, \cdots, n)$ yields

$$\frac{\partial E}{\partial S_i}=-\int_0^\infty [f(t)-f_D(t)]\, e^{-t/\tau_i} dt=0 \qquad (i=1, 2, \cdots, n) \tag{30}$$

This implies that

$$\hat{f}\left(\frac{1}{\tau_i}\right)=\hat{f}_D\left(\frac{1}{\tau_i}\right) \quad (i=1, 2, \cdots, n) \tag{31}$$

Substituting Eqs. (31) and (28) into Eq. (30), we can determine $S_j (j=1, 2, n)$ by solving

$$\sum_{j=1}^{n}\left(\int_0^\infty e^{-t/\tau_j} e^{-t/\tau_i} dt\right) S_j=\hat{f}\left(\frac{1}{\tau_i}\right) \quad (i=1, 2, \cdots, n) \tag{32}$$

For the stress relaxation problem in the homogenization analysis, the followings must be calculated by using the Schapery's method mentioned above:

(Homogenized viscoelastic coefficients)

$$\boldsymbol{M}^h(t)=\langle \boldsymbol{D}_0\rangle+\sum_{i=1}^{n}\langle \boldsymbol{D}_i\rangle \exp(-\tilde{\gamma}_i t) \tag{33}$$

$\langle \boldsymbol{D}_0\rangle$, $\langle \boldsymbol{D}_i\rangle$; Unknown coefficients

(Homogenized stress)

$$\langle \sigma_D(t)\rangle=\langle \sigma_1(\infty)\rangle+\sum_{i=1}^{n}\langle \boldsymbol{S}_i\rangle \exp(-\tilde{\gamma}_i t) \tag{34}$$

$\langle \boldsymbol{S}_i\rangle$: Unknown coefficients

$\langle \sigma_1(\infty)\rangle$: Averaged stress at $t=\infty$ calculated by using $G(\infty)$ and $K(\infty)$.

(Micro-stress)

$$\sigma_D(t)=\sigma_1(\infty)+\sum_{i=1}^{n}\boldsymbol{S}_i \exp(-\gamma_i t) \tag{35}$$

$\boldsymbol{S}_i$: Unknown coefficients

$\sigma_1(\infty)$: Micro-stress at $t=\infty$ calculated by using $G(\infty)$ and $K(\infty)$.

It can be proved that in the Schapery's method applied for the stress relaxation problem, the most efficient way is to set as

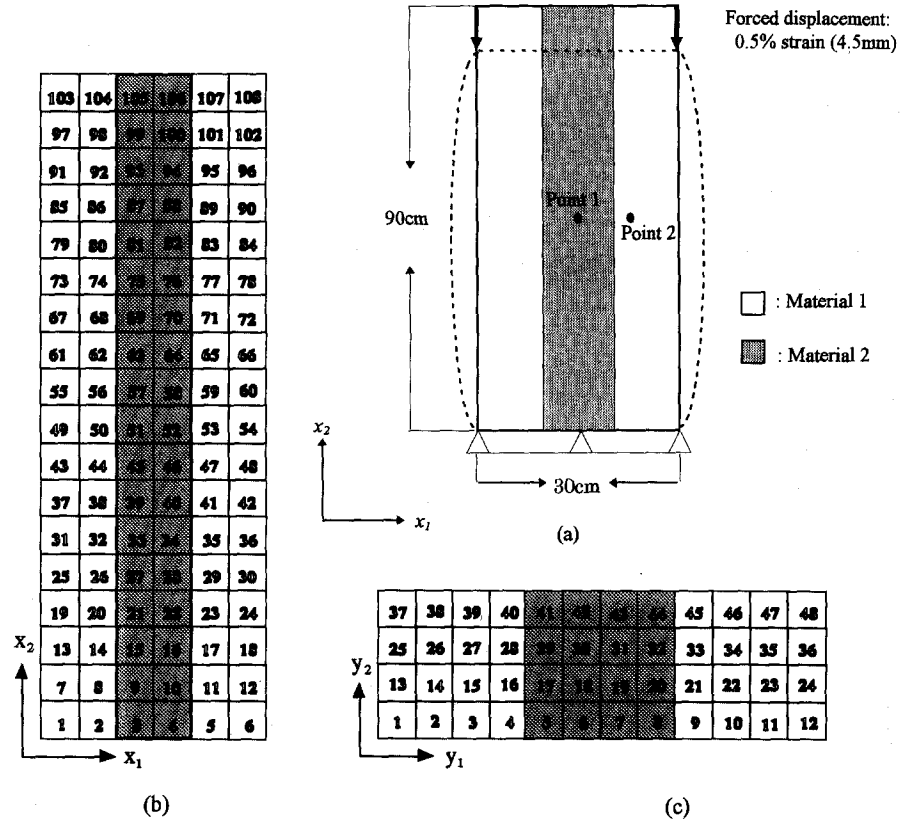

Fig. 7 (a) Model for the verification problem. (b) Finite element mesh for the conventional analysis and the global problem in homogenization analysis (the same mesh is used). (c) Mesh for the unit cell problem in homogenization analysis.

$$\gamma_i = \tilde{\gamma}_i = \frac{1}{\tau_i}$$

where τ_i is the relaxation times. Note that we here assumed $\tau_i^s = \tau_i^v$, but this is not essential.

3.4. Numerical examples

3.4.1. Verification problem

We first verify the proposed method by comparing with the conventional method for a simple two dimensional stress relaxation problem under plane strain condition (Fig. 7(a)). Note that in the conventional analysis a fine mesh of finite elements are used (Fig. 7(b)), while in the homogenization analysis, we can use a coase mesh but here the fine mesh same as the conventional analysis is employed. The finite element mesh for solving the unit cell problem is shown in Fig. 7(c). The material properties used are as follows:

(Material 1)

$$K(t) = 5.98 + 6.11\exp(-t/10.8) + 2.09\exp(-t/32.9)$$
$$G(t) = 5.06 + 5.17\exp(-t/10.8) + 1.77\exp(-t/32.9)$$

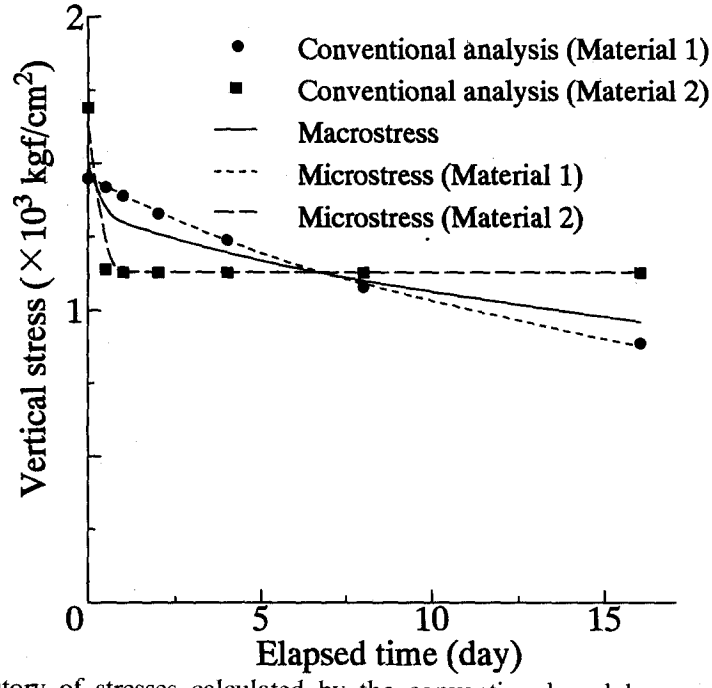

Fig. 8 Time history of stresses calculated by the conventional and homogenization analyses.

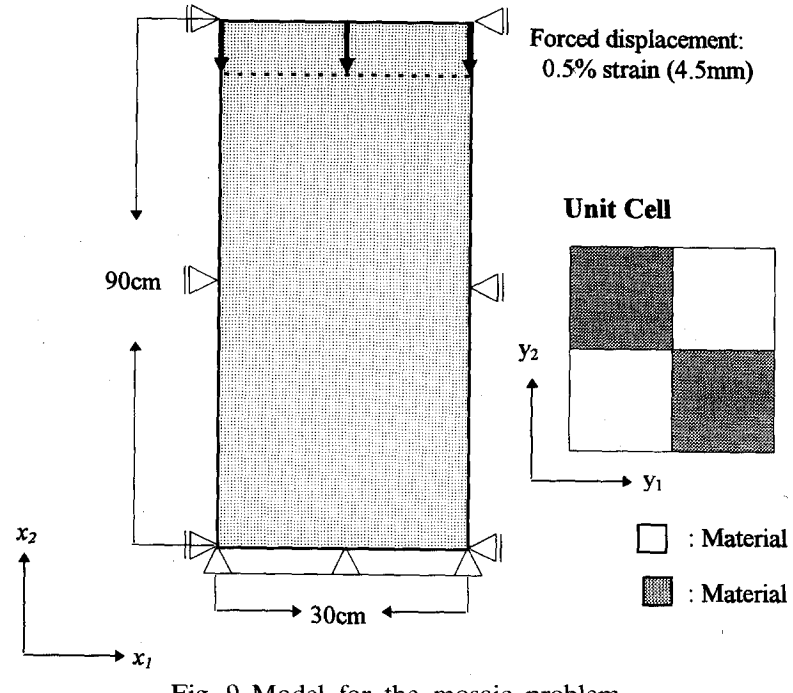

Fig. 9 Model for the mosaic problem.

(Material 2)

$$K(t)=12.0+4.0\exp(-t/0.0735)+2.0\exp(-t/0.1685)$$
$$G(t)=9.0+4.0\exp(-t/0.0735)+2.0\exp(-t/0.1685)$$

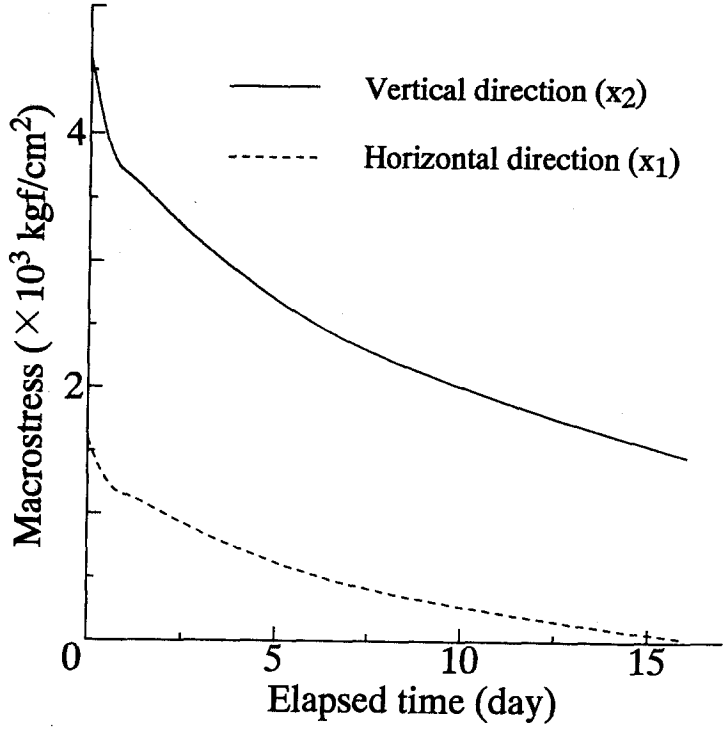

Fig. 10 Time history of macrostresses for the mosaic problem.

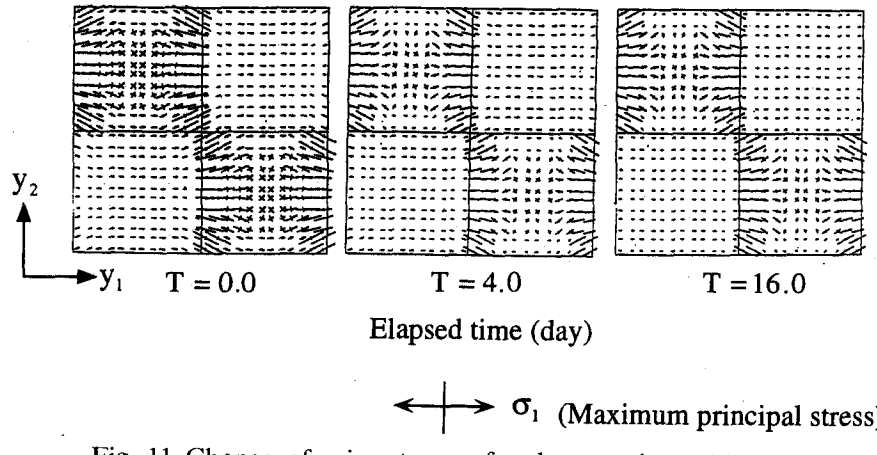

Fig. 11 Change of microstresses for the mosaic problem.

Fig. 8 shows the stress histories at the mid-point of the model (see Fig. 7(a)). We can find a good correspondence of the results of both analyses, and the homogenized stress shown by a solid line is in-between for the stresses developed in two materials.

3.4.1. Mosaic problem: Crystalline rock model

We next show results for a model of crystalline rock (Fig. 9). The unit cell is made by two

materials assuming feldspar and quartz. The material properties used are as follows:

(Material 1: feldspar)

$$K(t)=6.0+6.0\exp(-t/10)+2.0\exp(-t/30)$$
$$G(t)=5.0+5.0\exp(-t/10)+2.0\exp(-t/30)$$

(Material 2: quartz)

$$K(t)=120+20\exp(-t/0.05)+10\exp(-t/0.15)$$
$$G(t)=90+15\exp(-t/0.05)+8\exp(-t/0.15)$$

Fig. 10 shows the time histories of homogenized stresses at the mid-point of the model. The shear stress is not appeared in these homogenized stresses, while the micro-stresses are not uniformly distributed (Fig. 11). We should note that the homogenized stress may be useful to estimate the global distribution of stresses, but the micro-stress is quite fluctuating.

Aknowledgements

A part of this research was supported by Power Reactor and Nuclear Fuel Development Corporation under the contraction of PNC PJ1603 95-001.

References

Ahrens, T.J. and Rubin, A.M. (1993), "Impact-induced tensional failure in rock", *J. Geophys. Res.*, **98**, 1185-1203.

Birch, F. (1961), "The velocity of compressional waves in rocks to 10 kilobars, Part 2", *J Geophys. Res.*, **66**, 2199-2224.

Bombolakis, E.G. (1973), "Study of the brittle fracture process under uniaxial compression", *Tectonophysics*, **18**, 231-248.

Kern, H., and Wenk, H.-R. (1985), "Anisotropy in rocks and the geological significance", in *Preferred Orientation in Deformed Metals and Rocks: An Introduction to Modern Texture Analysis* (ed. H.-R. Wenk), Academic Pr., London, 537-555.

Kranz, R.L. (1979a), "Crack growth and development during creep of Barre granite", *Int. J. Rock Mech. Min. Sci. Geomech. Abstr.*, **16**, 23-35.

Kranz, R.L. (1979b), "Crack-crack and crack-pore interactions in stressed granite", *Int. J. Rock Mech. Min. Sci. Geomech. Abstr.*, **16**, 37-47.

Nur, A. and Simmons, G. (1970), "The origin of small cracks in igneous rocks", *Int. J. Rock Mech. Min. Sci.*, **20**, 307-314.

Olsson, W.A. (1974), "Grain size dependence of yield stress in marble", *J. Geophys. Res.*, **79**, 4859-4862.

Sanchez-Palencia, E. (1980), *Non-homogeneous media and vibration theory*, Springer-Verlag, Paris.

Schapery, R.A. (1961), "Approximate method of transform inversion for viscoelastic stress analysis", *Proc. 4th U.S. Nat. Cong. Applied Mech.*, 1075-1085.

Skinner, J.B. (1966), "Thermal expanssion", in *Handbook of Physical Constants*, ed. S.P. Clark, Mem. Geol. Soc. Am., **75**.

Wong, T.-F. (1990), "Effect of grain size on brittle and semibrittle strength: Implications for micromechanical modeling of failure in a compression", *J. Geophys. Res.*, **95**, 10907-10920.

Yukutake, H. (1989), "Fracturing process of granite inferred from measurements of spatial and temporal variations in velocity during triaxial deformations", *J. Geophys. Res.* **94**, 15639-15651.